ISSN 0038-0946, Solar System Research, 2025, Vol. 59:95. © Pleiades Publishing, Ltd., 2025.

Capabilities of the Sun-Terahertz Scientific Instrumentation Detectors in Registering Solar Radiation: Preliminary Evaluation from the Ground-Based Data

M. V. Philippov[a, *, **], V. S. Makhmutov[a], G. I. Kropotov[b], M. V. Razumeyko[a], E. D. Tulnikov[a], and S. V. Sokov[a]

[a] *Lebedev Physical Institute (LPI RAS), Russian Academy of Sciences, Moscow, 119911 Russia*

[b] *Tydex LLC, St. Petersburg, 194292 Russia*

**e-mail: mfilippov@frtk.ru*

***e-mail: filippovmv@lebedev.ru*

Received August 1, 2025; revised August 15, 2025; accepted August 18, 2025

Abstract—The paper describes the Sun-Terahertz space experiment planned for 2025–2027 onboard the Russian segment of the International Space Station (ISS). The main goals of the experiment are to obtain information on the terahertz radiation of the Sun, as well as to study active regions and solar flares. The scientific instrumentation of the Sun-Terahertz experiment contains eight channels (detectors) sensitive to radiation in a frequency range of 0.4–12.0 THz. The purpose of this study is to estimate the voltage at the output of scientific instrumentation detectors during the ISS onboard experiment from the ground-based measurement data and to determine minimal increases in the radiation flux reliably registered by the scientific instrumentation against the background of inherent noises.

Keywords: Sun, solar flares, terahertz radiation, optical system, Golay cell

DOI: 10.1134/S0038094625600635

INTRODUCTION

The Sun is a strong source of electromagnetic radiation in a wide range of frequencies and energies. Currently, ground-based and extra-atmospheric monitoring of solar radiation is carried out in almost the entire spectrum, from radio to gamma radiation (Kinnison et al., 2020; Howard et al., 2013; Domingo et al., 1995; Davila et al., 1996). However, the terahertz range remains the least studied, since it is almost completely absorbed by the terrestrial atmosphere. The exceptions are, first, the THz–mid-IR range at a frequency of about 15 THz (Giménez de Castro et al., 2020), within which the atmosphere is not completely opaque, especially at high altitudes where the water vapor content is substantially lower, and, second, the IR transparency window with a central frequency of about 30 THz (approximately 21–38 THz), through which the radiation can be registered (Kaufmann et al., 2015).

The Sun-Terahertz space experiment is primarily focused on a thorough study of solar radiation induced by flare activity in the terahertz range (Kalinin et al., 2021). The main goal of the experiment is to obtain new observation data that are necessary to construct and improve physical models of generating powerful solar proton flares and to develop methods for their operational forecasting (Kaufmann et al., 1985, 2001, 2003, 2004; Kaufmann, 1996; Krucker et al., 2013; Luthi et al., 2004; Makhmutov et al., 2003, 2011).

Studying flare activity at different frequencies allows us to investigate physical processes occurring at different levels of the solar atmosphere.

In the IR and subterahertz ranges, the radiation of both thermal (free–free emission) and nonthermal nature, associated with electron acceleration, is observed. Particularly, observations in the submillimeter range provide insight into the mechanisms of acceleration and transfer of high-energy electron flows in the lower layers of the atmosphere—from the transition region to the chromosphere (Wedemeyer et al., 2016). In a number of observations, the subterahertz radiation exhibits a spectral component that grows with frequency, which sharply distinguishes it from the classical synchrotron spectrum decreasing in the microwave range (Kontar et al., 2018). In some cases, the components, emitting exclusively in the subterahertz range and having no pronounced association with microwave bursts, are recorded, which indicates possible localized sources of high density and temperature (Kaufmann et al., 2004; Krucker et al., 2013). These anomalous spectral features suggest that it is necessary to study radiation in a range of higher terahertz frequencies.

Fig. 1. The scientific instrumentation of the Sun-Terahertz experiment when measuring the solar radiation.

To obtain new experimental data in a range of 1–10 THz is of high importance for determining the physical nature of the additional spectral component and for identifying the frequencies, at which the slope of the spectrum of solar flares changes. These data will make it possible to refine the parameters of sources and mechanisms generating radiation, as well as to improve predictive models of solar activity, including estimates of the probability and intensity of proton flares.

INSTRUMENTATION FOR THE SUN-TERAHERTZ EXPERIMENT

The Sun-Terahertz scientific instrumentation contains an electronics module and a block of eight detectors (channels) sensitive to radiation at frequencies of 0.4, 0.7, 1.0, 3.0, 5.0, 7.0, 10.0, and 12.0 THz (Philippov et al., 2024a). Each of the detectors consists of the following components: an optical telescope containing a large and a small mirror (Kvashnin et al., 2021); a system of filters (Kropotov et al., 2023) that includes a cut-off low-pass filter (LPF 23.1; https://www.tydexoptics.com/pdf/ru/THz_Low_Pass_Filter.pdf) and a band-pass filter (BPF; http://www.tydexoptics.com/ru/products/tgc-ustrojstva/thz_band_pass_filter/); an optical chopper (Philippov et al., 2023); a receiver, which is an optoacoustic converter (OAC)—the Golay cell—with an entrance window made of high-density polyethylene (HDPE; https://www.tydexoptics.com/ru/products/thz_optics/thz_materials/) (Kaufmann et al., 2014; Kropotov and Kaufmann, 2013; Philippov et al., 2024b); and an amplifier board.

The onboard implementation of the Sun-Terahertz space experiment is planned for 2026–2027.

MODEL OF ATMOSPHERIC ABSORPTION OF SOLAR RADIATION

To verify the functionality of the scientific instrumentation, the latter was installed on a specially constructed platform (Fig. 1). The measurements of solar radiation were carried out at the Dolgoprudny research station (DRS) of the LPI RAS.

To analyze the results of ground tests of a flight prototype of the scientific instrumentation, as well as to evaluate signals from the detectors receiving the quiet Sun radiation during the experiment onboard the ISS, it is necessary to take into account the influence of the atmosphere on the data of ground tests—the scattering and absorption, which is caused by a combination of the following basic mechanisms.

(1) The gaseous component of absorption resulting from absorption by molecules of atmospheric gases in their characteristic lines and bands, which is described by the HITRAN databases (Rothman, 2021).

(2) The Rayleigh scattering, which is the scattering of radiation on molecules, resulting from interaction of radiation with molecules of gases in the atmosphere (Rayleigh, 1871). The intensity of scattered radiation is inversely proportional to the fourth power of the wavelength: $I_R \sim 1/\lambda^4$.

(3) The absorption and scattering by particles (aerosols) (Bond and Bergstrom, 2006).

To calculate the gas component of atmospheric transmission with taking into account the altitude profiles of pressure, temperature, and gas concentration, one can use the HAPI library (Kochanov et al., 2016) and the standard atmosphere model (U.S. Standard Atmosphere, 1976).

The atmosphere was conditionally divided into layers corresponding to the heights h_i: 0, 500, 1000, 1500, 2000, 2500, 3000, 4000, 5000, 6000, 7000, 8000, 9000, 10000, 11000, 12000, 14000, 16000, 18000, 20000, 24000, 28000, 32000, 36000, 40000, 50000, 60000, 80000, and 100000 m. Hence, the thickness of the ith layer is defined as: $\Delta h_i = h_{i+1} - h_i$. In total, there are 28 layers.

For the altitude values specified, the values of the atmospheric pressure and temperature were obtained and the absorption spectra were calculated for molecules O_2, CO_2, CO, H_2O, N_2, CH_4, NO, NO_2, O_3, SO_2, N_2O, and their isotopes according to the standard atmosphere tables.

In the lower atmospheric layers, the mole fraction of H_2O, CO_2, and O_3 varies greatly with altitude, so the distribution of these gases in the atmosphere (an altitude profile) is taken into account. The mole fraction of the remaining molecules in the atmospheric gas mixture is assumed to be constant.

For molecules (or small particles) at the wavelengths significantly exceeding the size of particles, the scattering cross-section σ_R (expressed in cm^{-2}) can be written by a modified formula for the Rayleigh scattering (Sneep and Ubachs, 2005):

$$\sigma_R(\lambda) = \frac{24\pi^3\left(n^2-1\right)^2}{\lambda^4 N_c^2\left(n^2+2\right)^2}F, \quad (1)$$

where n is the refractive index of air ($n \approx 1.0003$); λ is the wavelength (expressed in centimeters); N_c is the standard molecular concentration of air under normal conditions ($N_c \approx 2.54 \times 10^{19}$ molecules/cm^3); and F is the depolarization factor ($F \approx 1$, since the geometry of molecules is ignored in these calculations).

For the ith layer, the concentration of air molecules N_{air}^i (molecules/cm^3) can be written as

$$N_{air}^i = \frac{P_i}{kT_i} \times 10^{-6}, \quad (2)$$

where k is the Boltzmann constant ($k = 1.38 \times 10^{-23}$ J/K); P_i is the atmospheric pressure (Pa) in the ith layer of air; and T_i is the temperature (K) of the ith layer of air.

The optical thickness of the ith layer of air is

$$\tau_i(\lambda) = \sigma_R(\lambda) N_{air}^i \Delta h_i \times 10^2. \quad (3)$$

According to the Bouguer–Lambert–Beer law, the resulting spectral coefficient of atmospheric transmission $t_R(\lambda)$ (relative units) is written as (Sivukhin, 2002)

$$t_R(\lambda) = e^{-\left(\sum_{i=0}^{27}\tau_i(\lambda)\right)}. \quad (4)$$

When passing through a medium containing particles (e.g., dust, water droplets, and aerosols), the electromagnetic radiation interacts with these particles, which results in scattering and absorption processes. The Mie theory (Bohren and Huffman, 1983) is an exact solution of Maxwell's equations for spherical particles with arbitrary sizes relative to the wavelength and with a complex refractive index $m = n + ik$, where n is the real part of the refractive index, which determines the speed of light propagation in a substance and influences the refraction and reflection of waves at the boundary between substances, and k is the absorption coefficient.

The Rayleigh scattering theory can be considered as a limiting case of the Mie theory for particles of small sizes. However, these two models are traditionally analyzed and applied separately, since the differences in scales of particles and in interaction physics are significant: the Rayleigh scattering is relevant for molecules and small aerosol particles, while the Mie theory is applied to particles comparable in size to the wavelength or larger, which requires not only the scattering but also the absorption to be accounted for.

To calculate the scattering and absorption with the Mie theory, the PyMieScatt library was used (Sumlin et al., 2017, 2018a, 2018b). The PyMieScatt package is designed to numerically simulate the scattering of electromagnetic waves on spherical particles and allows the scattering n and absorption k coefficients to be calculated.

A multifractional model of aerosols in the atmosphere, roughly corresponding to the conditions of a moderately polluted suburb (Hussein et al., 2008), has been developed. The model includes the following five characteristic fractions of particles, differing in size, molecular concentration in the near-surface layer, and chemical composition presumed (Li et al., 2023; Morakinyo et al., 2016).

— Ultrafine soot, which is particles with a radius of 0.005 μm and a concentration of 800 particles/cm^3. This fraction corresponds to agglomerates of elemental carbon produced during fuel combustion.

— Fine dust, which is particles with a radius of 0.03 μm and a concentration of 1000 particles/cm^3. Its possible components include inorganic salts (e.g., sulfates and nitrates) and mineral dust (silicon oxides and aluminum). These particles can be either primary (from road dust) or secondary, formed from precursor gases.

— Water droplets and secondary aerosols with a radius of 0.1 μm and a concentration of 600 particles/cm^3. These are hygroscopic particles containing ammonium salts and organic compounds, as well as liquid water droplets at high humidity. The main source is secondary organic aerosols (SOA) produced due to atmospheric photochemistry.

— Large particles (pollen, spores, and organic matter) with a radius of 0.7 μm and a concentration of 100 particles/cm^3. This fraction includes biological aerosols, as well as organic and mineral dust. It may contain cellulose, proteins, plant fragments, etc.

— Very large particles (construction dust; e.g., calcite $CaCO_3$) with a radius of 2.0 μm and a concentration of 2 particles/cm^3. This fraction includes cement dust, ash, abrasive materials, and heavy inorganic compounds. Its source is construction and road-repair work and mechanical destruction of materials.

The model takes into account dispersion (dependence on a wavelength of incident radiation) of the complex refractive index $m(\lambda)$ for each fraction (https://refractiveindex.info; Sumlin et al., 2018b; Malitson, 1965; Hale and Querry, 1973).

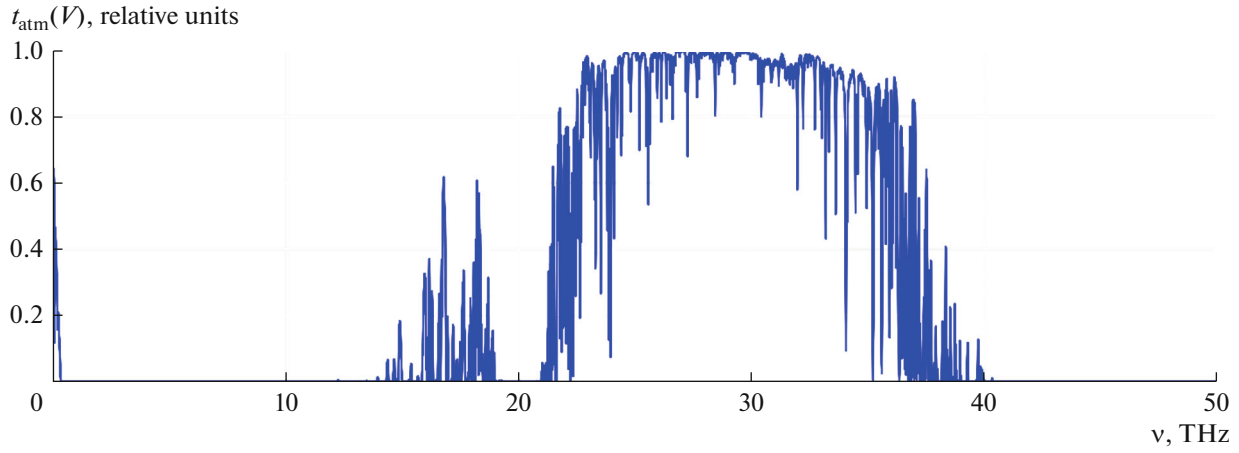

Fig. 2. The resulting spectral transmission coefficient of the atmosphere in a frequency range of 0.01–50 THz with a step of 0.01 THz.

The altitude profile of the aerosol concentration is accounted for by an exponential relationship that describes the decrease in the concentration of aerosol particles with increasing altitude. For each of the aerosol fractions, we specified a characteristic scale height (h_{sc} = 2500, 2000, 1500, 1000, and 500 m, respectively), which is a parameter that shows how high a given fraction can rise in the atmosphere (Hayasaka et al., 2007). This parameter makes it possible to take into account the physical properties peculiar for different particles: small and light particles (such as ultrafine soot) remain suspended at high altitudes, while heavy particles (such as construction dust) quickly settle and concentrate near the surface.

Hence, for the *i*th particle, the altitude profile of the aerosol concentration $N_i(h)$ (particles/cm^3) can be written as

$$N_i(h) = N_0^i e^{\frac{-h}{h_m^i}}, \quad (5)$$

where N_0^i is the concentration (particles/cm^3) assumed for the *i*th particle in the near-surface layer and h is the altitude above sea level (expressed in meters).

Figure 2 shows a diagram for the resulting spectral coefficient of the atmospheric transmission $t_{atm}(\nu)$ (relative units) in a frequency range of 0.01–50 THz. It takes into account the molecular absorption (the gaseous component) and the Rayleigh and aerosol (the Mie theory) scattering components calculated with the described model.

It should be noted that the result of applying the Mie theory to large, biologically complex objects (e.g., pollen or spores) is approximate because of their heterogeneous structure and nonspherical shape.

It is also worth noting that, in the operating frequency range of the scientific instrument detectors ($\nu < 30$ THz), the atmospheric transmission is mainly defined by molecular absorption.

To account for changes in the path of solar radiation through the atmosphere in dependence on the angle of observation, a concept of air mass M (relative units) is used; it is defined as a ratio of the path length of light through the atmosphere to the minimal path length corresponding to the Sun at its peak. In the simplest approximation, the air mass is calculated through the cosine of the zenith angle θ: $M(\theta) = 1/\cos(\theta)$.

For large zenith angles, a more complex empirical formula proposed by Kasten and Young (1989) is used:

$$M(\theta) = \frac{1}{\cos(\theta) + 0.50572 \times (96.07995 - \theta)^{-1.6364}}. \quad (6)$$

This formula takes into account the Earth's curvature and changes in the atmospheric density with altitude, which makes the result more accurate for angles close to the horizon. With the air mass concept, it is possible to correct for the transmission of light through the atmosphere, which is important for calculating the solar radiation at different observation angles. The air mass $M(\theta)$ grows with increasing zenith angle and reaches the maximum near the horizon (at $\theta = 90°$).

To correct the spectral coefficient of the solar radiation transmission through the atmosphere with accounting for the angle of observation, when the air mass $M(\theta)$ has been calculated, the following correction is introduced:

$$t_{atm}(\nu, \theta) = t_{atm}(\nu)^{M(\theta)}. \quad (7)$$

The zenith angle is determined using the Astropy library (https://www.astropy.org/) from the observer's geographical location and observation time.

THE LEVELS OF RECEIVER SIGNALS IN EIGHT DETECTING CHANNELS OF THE SCIENTIFIC INSTRUMENTATION UNDER CONDITIONS OF THE ISS ONBOARD EXPERIMENT: EVALUATION FROM THE GROUND-BASED MEASUREMENT DATA

A series of ground-based measurements of the background solar radiation with a flight model of the scientific instrumentation was carried out at the DRS LPI RAS on May 1, 2024. Further, in the data analysis, we use the measurements obtained between 14:17 and 14:32 Moscow time; consequently, to determine the angle θ, 11:25 (UTC) was selected as a time moment for the initial data. According to the calculations, $\theta = 46.10°$ and $M(\theta) = 1.44$.

The transmission coefficient of the optical path $t_{op}(\nu)$ (relative units) of the scientific instrumentation is presented by a general formula

$$t_{op}(\nu) = \rho_{tel}^2(\nu) t_{HDPE}(\nu) t_{LPF}(\nu) t_{BPF}(\nu) \mathrm{diff}(\nu), \quad (8)$$

where $\rho_{tel}^2(\nu)$ is the spectral reflection coefficient of the telescope; $t_{LPF}(\nu)$,$t_{BPF}(\nu)$, and $t_{HDPE}(\nu)$ are the spectral transmission coefficients of the band filter LPF 23.1, the cut-off filter BPF, and the HDPE entrance window, respectively; and $\mathrm{diff}(\nu)$ is the spectral coefficient characterizing the diffraction losses in the telescope (all of the listed quantities are expressed in relative units).

The resulting transmission coefficient $t_{res}(\nu, \theta)$ (relative units) of the whole system is an aggregate value that takes into account the losses at each step of the light path—from the atmosphere to the detector—including the influence of the zenith angle and the properties of the optical tract elements of the scientific instrumentation and the entrance window of the receiver:

$$t_{res}(\nu, \theta) = (t_{atm}(\nu))^{M(\theta)} t_{op}(\nu), \quad (9)$$

where $t_{atm}(\nu)$ (relative units) is the spectral transmission coefficient of the atmosphere that takes into account the absorption by molecules of gases, the Rayleigh scattering, and the absorption and scattering by particles (aerosols).

Then, with accounting for the influence of the atmosphere and the zenith angle, the spectral density of solar radiation coming to receivers of the scientific instrumentation is

$$L_{atm}(\nu, \theta) = r_{E490-22}(\nu) t_{res}(\nu, \theta), \quad (10)$$

where $r_{E490-22}(\nu)$ is the radiant emittance of the Sun (expressed in W/(m^2 Hz)) calculated with the ASTM E 490-22 model (https://www.astm.org/e0490-22.html).

Figure 3 shows a diagram for the spectral density of solar radiation for channel 5 (5.0 THz) at $\theta = 46.10°$. The red dashed line corresponds to the spectral density of radiation at the boundary of the atmosphere. The blue line corresponds to the spectral density of radiation with accounting for losses in the atmosphere. As can be seen, in the ground-based measurements, radiation from the non-target frequency range, roughly of 14 to 19 THz, mostly reaches the receiver. The cause of this is that molecules in the atmosphere almost completely absorb a lower-frequency component of the solar terahertz radiation, corresponding to the range from terahertz to mid-IR (Giménez de Castro et al., 2020). Hence, it can preliminarily be concluded that, under climatic conditions of Moscow, the terahertz radiation can be registered in a range of about 14–19 THz with the bandpass filters centered at a frequency near 15 THz and with the detectors similar to those used in the Sun-Terahertz scientific instrumentation. For the other channels, the diagrams are almost identical.

A signal of the terahertz detector located on the Earth and pointed towards the Sun contains the following components:

— the direct solar radiation, which is a target signal;

— the scattered solar radiation (re-radiated by the atmosphere), which is induced by interaction of solar radiation with molecules of air and water vapor and may contribute to the registered signal, especially at high humidity (Slocum et al., 2013);

— the thermal radiation of the Earth and atmosphere, which is a source of the background signal in the terahertz range; on average, the atmosphere (in the near-surface layer) and the Earth's surface emit as bodies with a temperature of ~288 K in a range of approximately 4–100 μm and with the spectral density maximum of radiation at about 15 μm (20 THz) (Petty, 2006).

To estimate the contribution of background radiation, a single-channel model of the detector (Fig. 4) was used. It was mounted on a rotating platform, which also housed a sensor of clouds based on an IR thermometer MLX90614 (https://www.melexis.com/en/product/mlx90614/digital-plug-play-infrared-thermometer-to-can). The measurements were performed with a differential method: first, the signal is registered when the detector is pointed at the Sun; then, to record the background atmospheric radiation, the detector is turned away from the Sun around a vertical axis at an angle of approximately 90°. The measurements were made sequentially for each of the channels by replacing the BPF bandpass filters. The duration of the experiment was about three hours.

Figure 5 shows a diagram for the receiver's signal measured in channel 6 (7.0 THz). The area, corresponding to the detector pointed at the Sun, is shown in orange. The blue area marks the plateau that corresponds to the detector turned away from the Sun at the

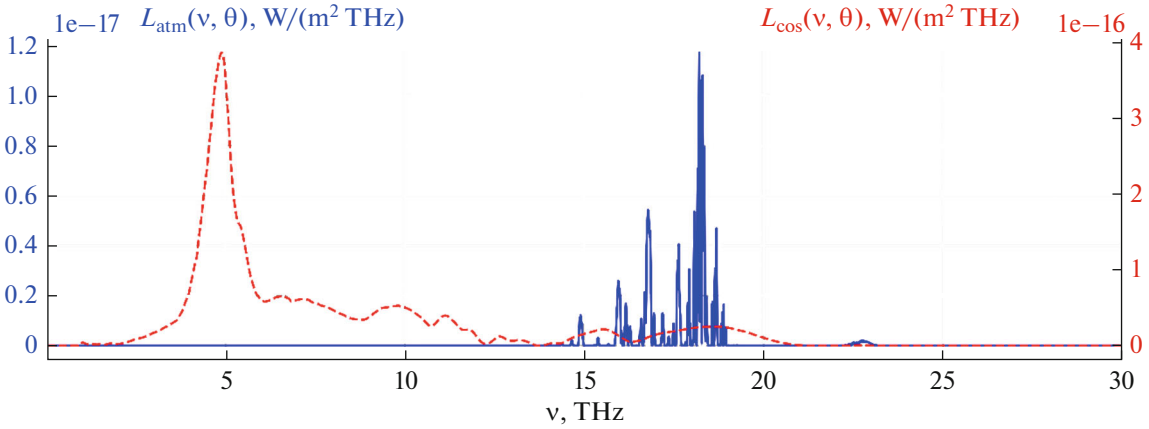

Fig. 3. The spectral density of solar radiation for channel 5 (5.0 THz) at $\theta = 46.10°$ in a frequency range of 0.01–30 THz with a step of 0.01 THz. The red dashed line shows the spectral density of radiation at the boundary of the atmosphere. The blue line corresponds to the spectral density of radiation with accounting for losses in the atmosphere.

Fig. 4. The instruments to measure the background radiation of the atmosphere. They are mounted on a rotating platform: a single-channel model of the detector (1) and the sensor of clouds (2).

initial time moment. The range between these areas corresponds to the measurements during the platform rotation. Since the OAC is extremely sensitive to vibrations, signal spikes are observed in this range. Further, the signal begins to decline gradually. This is probably caused by cooling the detector's components, which are also a source of radiation. As a result of the turning, the heat is redistributed to the other surfaces of the detector; and after a while the signal will begin to increase.

Thus, to estimate the relative magnitude of solar radiation, the average values of the signal in the orange and blue areas were used, as shown in Fig. 5.

In Table 1 we present the results of calculations of the contribution of solar radiation to the signal registered by the scientific instrumentation at the edge of

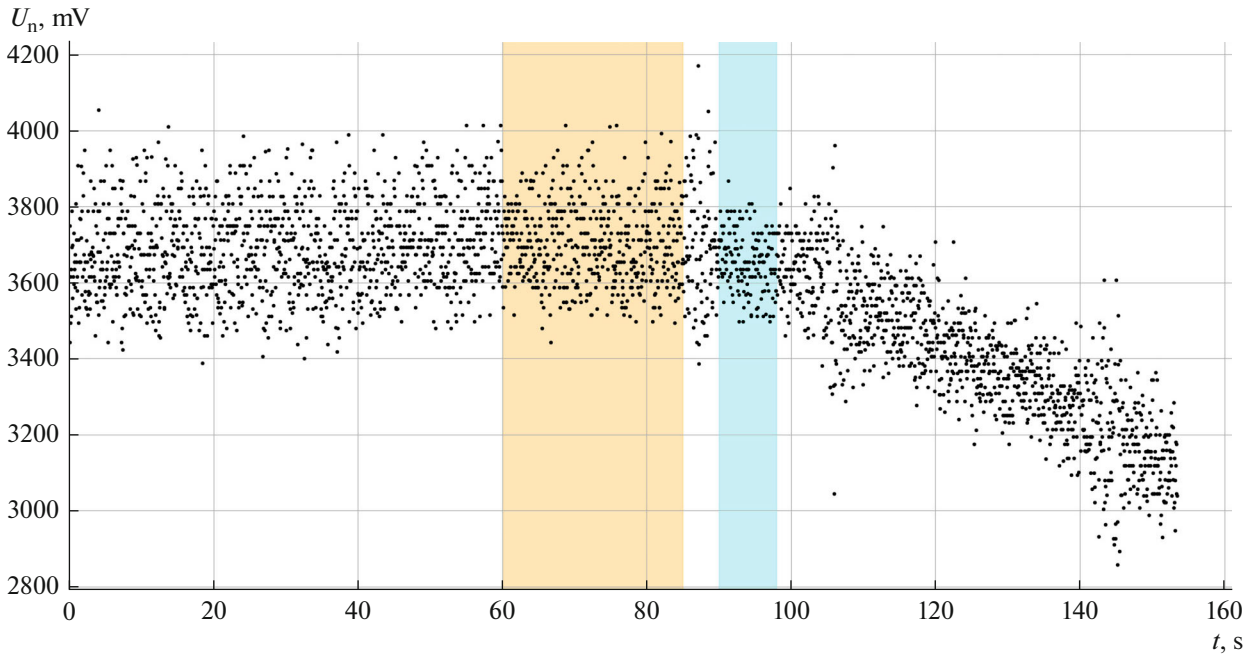

Fig. 5. The signal of the receiver within a detector of the single-channel model: the areas corresponding to the positions of the detector pointed at the Sun and turned away from the Sun are shown in orange and blue, respectively.

the atmosphere and in the ground-based experiment. The columns contain the following quantities: ν_{max} (THz) is the central frequency of transmission of the optical path in a given channel; U_{n1} and U_{n2} (W) are the average signals of the receiver pointed at the Sun and turned away from the Sun, respectively; $\alpha = 1 - U_{n1}/U_{n2}$ is the estimate of the fraction of solar radiation in the detectors (expressed in relative units); and T_{sky} (°C) is the effective brightness temperature of the sky according to the data of the cloud sensor, which serves as an inverse measure of the transparency of the atmosphere in the IR range. This parameter is an integral quantity that depends on many factors, including the temperature profile of the atmosphere, water vapor content, cloud cover, aerosols, etc. Consequently, the effective brightness temperature of the sky is only an approximate indicator.

Since there was no cloud cover during the measurements, the increase in T_{sky} is probably associated with accumulation of water vapor in the lower atmospheric layers and/or with the presence of a faint aerosol haze, which leads to a decrease in the atmospheric transparency in the IR range.

It can be concluded that, during the experiment, the weather conditions gradually deteriorated, which could lead, in particular, to somewhat underestimated results of the measurements in channels 7 and 8 compared to those in channel 1.

In Table 2 we show the results of calculations of the solar radiation fluxes reaching the receivers of the sci-

Table 1. The estimates of the solar radiation contribution to the signal of the scientific instrumentation under conditions of the ground-based experiment

Channel number	ν_{max}, THz	U_{n1}, W	U_{n2}, W	α, rel. units	T_{sky}, °C
1	0.40	2348.080	2302.038	0.020	5.56 ± 2.50
2	0.68	1443.476	1428.382	0.010	7.00 ± 2.77
3	0.98	1965.141	1926.752	0.020	7.08 ± 1.09
4	2.90	2905.569	2871.915	0.012	7.05 ± 0.63
5	4.84	3631.540	3548.684	0.023	9.93 ± 3.16
6	6.61	3702.962	3656.995	0.022	9.21± 3.00
7	9.69	2899.051	2886.985	0.004	10.80 ± 3.34
8	11.16	3893.515	3867.572	0.007	12.49 ± 3.46

Table 2. The results of calculations of the solar radiation fluxes reaching the scientific instrumentation receivers at the boundary of the atmosphere and under conditions of the ground-based experiment

Channel number	ν_{max}, THz	$\Phi_{cosm}(\nu)$, W	$\Phi_{atm}(\nu,\theta)$, W	β, rel. units	U_{atm}, mV	U_{cosm}, mV	U_{noise}, mV	γ, %
1	0.40	4.01×10^{-7}	4.74×10^{-9}	84.62	344.94	583.78	2.22	0.38
2	0.68	2.73×10^{-7}	3.71×10^{-9}	73.45	1144.85	840.89	2.15	0.26
3	0.98	3.57×10^{-7}	5.70×10^{-9}	62.66	734.07	919.94	2.15	0.23
4	2.90	1.02×10^{-6}	6.77×10^{-9}	151.21	940.85	1707.19	1.92	0.11
5	4.84	3.13×10^{-6}	1.54×10^{-8}	203.52	519.31	2430.87	2.22	0.09
6	6.61	3.61×10^{-6}	1.30×10^{-8}	277.50	478.36	2920.39	2.15	0.07
7	9.69	3.13×10^{-6}	1.49×10^{-8}	210.23	819.32	1033.47	2.15	0.21
8	11.16	3.23×10^{-6}	2.46×10^{-8}	131.39	436.19	401.18	1.92	0.48

entific instrumentation at the edge of the atmosphere and in the ground-based experiment. ν_{max} (THz) is the central frequency of the optical path transmission in a given channel. $\Phi_{cosm}(\nu)$ (Watts) is the solar radiation flux reaching the receiver of the scientific instrumentation at the edge of the atmosphere during the orbital flight; it was calculated for a frequency range from $\nu_1 = 0.01$ THz to $\nu_2 = 2000$ THz with the following formula

$$\Phi_{cosm} = S_{tel}\int_{\nu_1}^{\nu_2} r_{ASTM\ E}(\nu)\, t_{op}(\nu)\, d\nu. \qquad (11)$$

$\Phi_{atm}(\nu,\theta)$ (W) is the solar radiation flux coming to the receiver of the scientific instrumentation, which includes the contribution of the effects of the atmosphere and zenith angle. It was calculated for a range of frequencies from $\nu_1 = 0.01$ THz to $\nu_2 = 2000$ THz with formula (12). $\beta = \Phi_{cosm}(\nu)/\Phi_{atm}(\nu,\theta)$ is the calculated ratio of the solar radiation fluxes coming to the detectors at the edge of the atmosphere and in the ground-based measurements. U_{atm} (mV) is the receivers' signal during ground-based measurements of the background signal from the Sun according to the data for a period of 14:17–14:32 (Moscow time) on May 1, 2024. The measured values of the receivers' signal were corrected for the temperature effects (Philippov et al., 2024b), while the resulting value of U_{atm} was obtained by averaging the data over a time period specified. $U_{cosm} = \alpha\beta U_{atm}$ is the estimate (mV) of the signal of receivers in the flight model of the scientific instrumentation.

$$\Phi_{atm}(\nu,\theta) = S_{tel}\int_{\nu_1}^{\nu_2} r_{ASTM\ E}(\nu)\, t_{res}(\nu,\theta)\, d\nu. \qquad (12)$$

U_{noise} is the magnitude of inherent noises measured at the receiver output (Philippov et al., 2025) and corrected for the transfer characteristic of the electronics board, which was selected for each of the channels of the scientific instrumentation (Philippov et al., 2024a). $\gamma = \frac{U_{noise}}{U_{cosm}} \times 100\%$ is a ratio of the inherent noises of a receiver to the background signal from the Sun. Since for reliable detection the contribution of the flare component U_{flare} to the signal in the receiver should exceed its inherent noises, $\frac{U_{flare}}{U_{noise}} > 1$; consequently, γ can be considered as an estimate of the minimal flare signal registered in a specified channel.

The paper by Kontar et al. (2018) examines anomalous spectra of solar flares in a subterahertz range of 0.2–0.4 THz on the basis of the data from the Solar Submillimeter Telescope (SST), in which an increase in the intensity is observed with increasing frequency (Kaufmann et al., 2004). During solar flares of class X, the radiation flux may grow up to $(1-5) \times 10^4$ SFU (1 SFU = 10^{-22} W/(m^2 Hz)) at a frequency of 0.4 THz. Such significant increases in the radiation flux cannot be explained solely by braking radiation (Bremsstrahlung). In this regard, various nonthermal mechanisms are considered. Fleishman and Kontar (2010) proposed alternative sources of the subterahertz component, including synchrotron radiation of relativistic particles, as well as diffusion and Cherenkov radiation. Silva et al. (2007) showed that, in some X-class flares, the subterahertz component correlates with the high-energy X-ray radiation, which argues in favor of synchrotron radiation from nonthermal electrons. On the other hand, Kontar et al. (2018) proposed a model of thermal free-free emission from flare ribbons with temperatures of 10^4–10^6 K, which can reproduce a spectrum increasing with frequency. In the paper by Trottet et al. (2015), with the example of a flare on March 13, 2012, it was shown that the main part of radiation at a frequency of 30 THz is thermal, but this emission is a consequence of plasma heating by a stream of nonthermal particles.

According to the ASTM E 490-22 model, the radiation flux from the quiet Sun is $\Phi_{\text{ASTM E}}(0.4\ \text{THz}) \approx 208000$ SFU, while the ratio $\delta = \frac{\Phi_{\text{flare}}(0.4\ \text{THz})}{\Phi_{\text{ASTM E}}(0.4\ \text{THz})} \times 100\%$ reaches 24% in this case. With taking into account the estimate for γ, the minimal possible value of δ reliably recorded by the scientific instrumentation is 790 SFU. Since there are no experimental data for a frequency range of 0.8–12.0 THz, possible fluxes in the other channels of the scientific instrumentation during flare activity cannot be estimated.

CONCLUSIONS

The data of ground-based calibrations of the Sun-Terahertz scientific instrumentation were used to estimate the signals of receivers during the orbital experiment. The calculation of the atmospheric absorption includes consideration of the molecular absorption (the main contribution), the Rayleigh scattering, the scattering described by the Mie theory, as well as the zenith angle of the Sun. It should be noted that, when the Sun-Terahertz experiment is carried out under the Earth's conditions, the detectors of the scientific instrumentation are mainly calibrated by the radiation in a range of about 14–19 THz, since the target radiation in a frequency range of 0.4–12 THz contributes virtually nothing to the receivers' signal due to the characteristics of the detectors and the transmission spectrum of the atmosphere.

To estimate the contribution of solar radiation to the signal of the scientific instrumentation during ground-based calibrations against the background radiation from the atmosphere, we used a single-channel model of the detector mounted on a rotating platform. Measurements were performed with the differential method.

The minimal increases in the radiation fluxes from the Sun, which were reliably registered by the scientific instrumentation with taking into account inherent noises of the receivers, were evaluated (they exceeded the inherent noises at the output of scientific instrumentation receivers). Under conditions of the orbital experiment, the signal recorded due to a solar flare or an active region must exceed a characteristic magnitude of 0.07–0.48% of the quiet Sun radiation, depending on the frequency of a detecting channel. It is worth noting that, in the above calculations, the sensitivity of the scientific instrumentation was evaluated at a preliminary level, and its actual characteristics may differ significantly from those calculated, since it is impossible to take into account all influencing factors when interpreting the results of atmospheric measurements in application to future extra-atmospheric measurements.

The above results are of interest for future ground-based terahertz observations, especially in the atmospheric windows.

FUNDING

This work was financed from the LPI RAS budget. No additional grants were received to support this research.

CONFLICT OF INTEREST

The authors of this work declare that they have no conflicts of interest.

REFERENCES

Bohren, C.F. and Huffman, D.R., *Absorption and Scattering of Light by Small Particles,* New York: Wiley, 1983.

Bond, T.C. and Bergstrom, R.W., Light absorption by carbonaceous particles: An investigative review, *Aerosol Sci. Technol.,* 2006, vol. 40, no. 1, pp. 27–67. https://doi.org/10.1080/02786820500421521

Davila, J.M., Rust, D.M., Pizzo, V.J., and Liewer, P.C., Solar Terrestrial Relations Observatory (STEREO), in *Proc. SPIE's 1996 Int. Symp. Optical Sci. Engineering and Instrumentation,* 1996, vol. 2804. https://doi.org/10.1117/12.259724

Domingo, V., Fleck, B., and Poland, A.I., SOHO: The Solar and Heliospheric Observatory, *Space Sci. Rev.,* 1995, vol. 72, pp. 81–84. https://doi.org/10.1007/BF00768758

Fleishman, G.D. and Kontar, E.P., Sub-THz radiation mechanisms in solar flares, *Astrophys. J. Lett.,* 2010, vol. 709, no. 2, pp. L127–L132. https://doi.org/10.1088/2041-8205/709/2/L127

Giménez de Castro, C.G., Raulin, J.P., Valio, A., Alaia, G., Alvarenga, V., Bortolucci, E.C., Fernandes, S.H., Francile, C., Giorgetti, T., Kudaka, A.S., López, F.M., and 3 co-authors, HATS: A ground-based telescope to explore the THz domain, *Sol. Phys.,* 2020, vol. 295, no. 4, p. 56. https://doi.org/10.1007/s11207-020-01621-3

Hale, G.M. and Querry, M.R., Optical constants of water in the 200-nm to 200-μm wavelength region, *Appl. Opt.,* 1973, vol. 12, no. 3, pp. 555–563. . https://doi.org/10.1364/AO.12.000555

Hayasaka, T., Murayama, T., Shimizu, A., and Sugimoto, N., Vertical distribution and optical properties of aerosols observed over Japan during the Atmospheric Brown Clouds–East Asia Regional Experiment 2005, *J. Geophys. Res.: Atmos.,* 2007, vol. 112, no. D22, p. D22S35. https://doi.org/10.1029/2006JD008086

Howard, R.A., Vourlidas, A., Korendyke, C.M., Plunkett, S.P., Carter, M.T., Wang, D., Rich, N., Lynch, S., Thurn, A., Socker, D.G., and 37 co-authors, The solar and heliospheric imager (SoloHI) instrument for the Solar Orbiter mission, *Sol. Phys. Space Weather Instrum.,* 2013, vol. 8862, p. 88620H. https://doi.org/10.1117/12.2027657

Hussein, T., Martikainen, J., Junninen, H., Sogacheva, L., Wagner, R., Dal Maso, M., Riipinen, I., Aalto, P.P., and Kulmala, M., Observation of regional new particle

formation in the urban atmosphere, *Tellus B: Chem. Phys. Meteorol.,* 2008, vol. 60, no. 4, pp. 509–521. https://doi.org/10.1111/j.1600-0889.2008.00365.x

Kalinin, E.V., Philippov, M.V., Makhmutov, V.S., Maksumov, O.S., Stozhkov, Yu.I., Kvashnin, A.A., Izmailov, G.N., and Ozolin, V.V., A study of the characteristics of a terahertz radiation detector for the Solntse–Terahertz scientific apparatus, *Cosmic Res.,* 2021, vol. 59, no. 1, pp. 1–5. https://doi.org/10.1134/S0010952521010032

Kasten, F. and Young, P.J., Revised optical air mass tables and approximation formula, *Appl. Opt.,* 1989, vol. 28, no. 22, pp. 4735–4738. doi https://doi.org/10.1364/AO.28.004735

Kaufmann, P., Raullin, J.-P., de Castro, C.G.G., Levato, H., Gary, D.E., Costa, J.E.R., Marun, A., Pereyra, P., Silva, A.V.R., and Correia, E., A new solar burst spectral component emitting only in the terahertz range, *Astrophys. J.,* 2004, vol. 603, pp. L121–L124. https://doi.org/10.1086/383186

Kaufmann, P., Correia, E., Costa, J.E.R., Zodi Vaz, A.M., and Dennis, B.R., Solar burst with millimetre-wave emission at high frequency only, *Nature,* 1985, vol. 313, pp. 380–382. https://doi.org/10.1038/313380a0

Kaufmann, P., Submillimeter/IR solar bursts from high energy electrons, *AIP Conf. Proc.,* 1996, vol. 374, pp. 379–392. https://doi.org/10.1063/1.50945

Kaufmann, P., Costa, J.E.R., Gimenez De Castro, C.G., Hadano, Y.R., Kingsley, J.S., Kingsley, R.K., Levato, H., Marun, A., Raulin, J.-P., Rovira, M., Correia, V., and Silva, A.V.R., The new submillimeter-wave solar telescope, in *Proc. 2001 SBMO/IEEE MTT-S Int. Microwave Optoelectron. Conf.,* 2001, pp. 439–442. https://doi.org/10.1109/SBMOMO.2001.1008800

Kaufmann, P., Castro, C.G.G., Makhmutov, V.S., Raulin, J.-P., Schwenn, R., Levato, H., and Rovira, M., Launch of solar coronal mass ejections and submillimeter pulse bursts, *J. Geophys. Res.,* 2003, vol. 108, no. A7, p. 1280. https://doi.org/10.1029/2002JA009729

Kaufmann, P., Marcon, R., Abrantes, A., Bortolucci, E.C., Fernandes, L.O.T., Kropotov, G.I., Kudaka, A.S., Machado, N., Marun, A., Nikolaev, V., and 3 co-authors, THz photometers for solar flare observations from space, *Exp. Astron.,* 2014, vol. 37, pp. 579–598. https://doi.org/10.1007/s10686-014-9389-y

Kaufmann, P., White, S.M., Marcon, R., Kudaka, A.S., Cabezas, D.P., Cassiano, M.M., Francile, C., Fernandes, L.O.T., Hidalgo Ramirez, R.F., Luoni, M., and 3 co-authors, Bright 30 THz impulsive solar bursts, *J. Geophys. Res.: Space Phys.,* 2015, vol. 120, pp. 4155–4163. https://doi.org/10.1002/2015JA021313

Kinnison, J., Vaughan, R., Hill, P., Raouafi, N., Guo, Y., and Pinkine, N., Parker Solar Probe: A mission to touch the Sun, in *IEEE Aerosp. Conf.,* 2020, pp. 1–14. https://doi.org/10.1109/AERO47225.2020.9172703

Kochanov, R.V., Gordon, I.E., Rothman, L.S., Wcislo, P., Hill, C., and Wilzewski, J.S., HITRAN Application Programming Interface (HAPI): A comprehensive approach to working with spectroscopic data, *J. Quant. Spectrosc. Radiat. Transfer,* 2016, vol. 177, pp. 15–30. https://doi.org/10.1016/j.jqsrt.2016.03.005

Kontar, E.P., Motorina, G.G., Jeffrey, N.L.S., Tsap, Y.T., Fleishman, G.D., and Stepanov, A.V., Frequency rising sub-THz emission from solar flare ribbons, *Astron. Astrophys.,* 2018, vol. 620, p. A95. . https://doi.org/10.1051/0004-6361/201834124

Kropotov, G. and Kaufmann, P., THz photometers for solar flare observations from space, *Fotonika,* 2013, vol. 5, no. 41, pp. 40–50.

Kropotov, G.I., Shakhmin, A.A., Kaplunov, I.A., and Rogalin, V.E., Application of spectral devices in the optical engineering and scientific research, *Fotonika,* 2023, vol. 5, no. 17, pp. 378–393. https://doi.org/10.22184/1993-7296.FRos.2023.17.5.378.392

Krucker, S., Castro, C.G.G., Hudson, H.S., Trottet, G., Bastian, T.S., Hales, A.S., Kašparová, J., Klein, K.-L., Kretzschmar, M., Lüthi, T., and 3 co-authors, Solar flares at submillimeter wavelengths, *Astron. Astrophys. Rev.,* 2013, vol. 21, p. 58. https://doi.org/10.1007/s00159-013-0058-3

Kvashnin, A.A., Logachev, V.I., Filippov, M.V., Makhmutov, V.S., Maksumov, O.S., Stozhkov, Yu.I., Kalinin, E.V., Orlov, A.A., Ozolin, V.V., Izmailov, G.N., Krivolapova, O.Yu., and Gaifutdinova, A.G., Optical system design of the detector for solar terahertz emission measurements, *Kosm. Tekh. Tekhnol.,* 2021, vol. 4, no. 35, pp. 22–30. https://www.elibrary.ru/hgxxgn.

Li, Q.-Q., Guo, Y.-T., Yang, J.-Y., and Liang, C.-S., Review on main sources and impacts of urban ultrafine particles: Traffic emissions, nucleation, and climate modulation, *Atmos. Environ.: X,* 2023, vol. 9, p. 100221. https://doi.org/10.1016/j.aeaoa.2023.100221

Luthi, T., Magun, A., and Miller, M., First observation of a solar X-class flare in the submillimeter range with KOSMA, *Astron. Astrophys.,* 2004, vol. 415, pp. 1123–1132. https://doi.org/10.1051/0004-6361:20034624

Makhmutov, V.S., Raulin, J.P., Castro, C.G.G., Kaufmann, P., and Correia, E., Wavelet decomposition of submillimeter solar radio bursts, *Sol. Phys.,* 2003, vol. 218, pp. 211–220. https://doi.org/10.1023/B:SOLA.0000013047.26419.33

Makhmutov, V.S., Kurt, V.G., Yushkov, B.Yu., Grechnev, V.V., Kaufmann, P., Raulin, J.-P., Bazilevskaya, G.A., and Stozhkov, Yu.I., Spectral peculiarities of high energy X-ray radiation, gamma radiation, and Submillimeter radio emission in the impulsive phase of a solar flare, *Bull. Russ. Acad. Sci. Phys.,* 2011, vol. 75, no. 6, pp. 747–750.

Malitson, I.H., Interspecimen comparison of the refractive index of fused silica, *J. Opt. Soc. Am.,* 1965, vol. 55, no. 10, pp. 1205–1209. https://doi.org/10.1364/JOSA.55.001205

Morakinyo, O.M., Mokgobu, M.I., Mukhola, M.S., and Hunter, R.P., Health outcomes of exposure to biological and chemical components of inhalable and respirable particulate matter, *Int. J. Environ. Res. Public Health,* 2016, vol. 13, no. 6, p. 592. https://doi.org/10.3390/ijerph13060592

Petty, G.W., *A First Course in Atmospheric Radiation,* Madison: Sundog Publishing, 2006.

Philippov, M.V., Makhmutov, V.S., Maksumov, O.S., Kvashnin, A.A., Kalinin, E.V., Logachev, V.I., Gaifutdinova, A.G., Krivolapova, O.Yu., Sokov, S.V., and Mizin, S.V., A study of thermal effect of resonant optical shutters in space scientific equipment, *Space Eng. Technol.,* 2023, vol. 40, no. 1, pp. 8–18. https://www.elibrary.ru/wzamjn.

Philippov, M.V., Makhmutov, V.S., Maksumov, O.S., Kvashnin, A.A., Kvashnin, A.N., Razumeyko, M.V., Logachev, V.I., Mizin, S.V., and Sokov, S.V., Electronics unit for "Sun–Terahertz" scientific equipment, *Instrum. Exp. Tech.,* 2024a, vol. 67, pp. 545–553.

Philippov, M.V., Makhmutov, V.S., and Razumeyko, M.V., Scientific equipment for the Sun-Terahertz space experiment: Study of the temperature effect in the Golay cell, *Meas. Tech.,* 2024b, vol. 67, pp. 195–202. https://doi.org/10.1007/s11018-024-02335-9

Philippov, M.V., Makhmutov, V.S., Razumeyko, M.V., Kropotov, G.I., and Nikolaev, V.A., Method of checking the spectral sensitivity of optical paths of the Sun-Terahertz scientific instrumentation in the frequency range 0.4–20 THz, *Sol. Syst. Res.,* 2025, vol. 59, p. 26. https://doi.org/10.1134/S0038094624601683

Rayleigh, J.W., On the light from the sky, its polarization and color, *Philos. Mag.*, 1871, vol. 41, no. 4, pp. 107–120.

Rothman, L.S., History of the HITRAN Database, *Nat. Rev. Phys.,* 2021, vol. 3, pp. 302–304. https://doi.org/10.1038/s42254-021-00309-2

Silva, A.V.R., Share, G.H., Murphy, R.J., Costa, J.E.R., Giménez de Castro, C.G., Raulin, J.-P., and Kaufmann, P., Evidence that synchrotron emission from nonthermal electrons produces the increasing submillimeter spectral component in solar flares, *Sol. Phys.,* 2007, vol. 245, no. 2, pp. 311–326. https://doi.org/10.1007/s11207-007-9044-0

Sivukhin, D.V., *Obshchii kurs fiziki* (General Course of Physics), vol. 4: *Optika* (Optics), Moscow: Fizmatlit MFTI, 2002.

Slocum, D.M., Slingerland, E.J., Giles, R.H., and Goyette, T.M., Atmospheric absorption of terahertz radiation and water vapor continuum effects, *J. Quant. Spectrosc. Radiat. Transfer,* 2013, vol. 127, pp. 49–63. https://doi.org/10.1016/j.jqsrt.2013.04.022

Sneep, M. and Ubachs, W., Direct measurement of the Rayleigh scattering cross section in various gases, *J. Quant. Spectrosc. Radiat. Transfer,* 2005, vol. 92, no. 3, pp. 293–310. https://doi.org/10.1016/j.jqsrt.2004.07.025

Sumlin, B.J., Pandey, A., Walker, M.J., Pattison, R.S., Williams, B.J., and Chakrabarty, R.K., Atmospheric photooxidation diminishes light absorption by primary brown carbon aerosol from biomass burning, *Environ. Sci. Technol. Lett.,* 2017, vol. 4, no. 12, pp. 540–545. https://doi.org/10.1021/acs.estlett.7b00393

Sumlin, B.J., Heinson, W.R., and Chakrabarty, R.K., Retrieving the aerosol complex refractive index using PyMieScatt: A Mie computational package with visualization capabilities, *J. Quant. Spectrosc. Radiat. Transfer,* 2018a, vol. 205, pp. 127–134. https://doi.org/10.1016/j.jqsrt.2017.10.012

Sumlin, B.J., Heinson, Y.W., Shetty, N., Pandey, A., Pattison, R.S., Baker, S., Hao, W.M., and Chakrabarty, R.K., UV–Vis–IR spectral complex refractive indices and optical properties of brown carbon aerosol from biomass burning, *J. Quant. Spectrosc. Radiat. Transfer,* 2018b, vol. 206, pp. 392–398. https://doi.org/10.1016/j.jqsrt.2017.12.009

Trottet, G., Raulin, J.-P., Mackinnon, A., Giménez de Castro, G., Simões, P.J.A., Cabezas, D., de La Luz, V., Luoni, M., and Kaufmann, P., Origin of the 30 THz emission detected during the solar flare on 2012 March 13 at 17:20 UT, *Sol. Phys.,* 2015, vol. 290, no. 10, pp. 2809–2826. https://doi.org/10.1007/s11207-015-0782-0

U.S. Standard Atmosphere, Washington, D.C.: U.S. Government Printing Office, 1976.

Wedemeyer, S., Bastian, T., Brajša, R., Hudson, H., Fleishman, G., Loukitcheva, M., Fleck, B., Kontar, E.P., De Pontieu, B., Yagoubov, P., and 28 co-authors, Solar science with the Atacama Large Millimeter/Submillimeter Array—a new view of our Sun, *Space Sci. Rev.,* 2016, vol. 200, pp. 1–73. https://doi.org/10.1007/s11214-015-0229-9

Translated by E. Petrova